Published OnlineFirst June 19, 2020; DOI: 10.1158/0008-5472.CAN-19-2416

Extracellular-Regulated Protein Kinase 5-Mediated Control of p21 Expression Promotes Macrophage Proliferation Associated with Tumor Growth and Metastasis

Emanuele Giurisato[1,2], Silvia Lonardi[3], Brian Telfer[4], Sarah Lussoso[1], Blanca Risa-Ebri[2], Jingwei Zhang[2], Ilaria Russo[5,6], Jinhua Wang[7,8], Annalisa Santucci[1], Katherine G. Finegan[4], Nathanael S. Gray[7,8], William Vermi[3,9], and Cathy Tournier[2]

ABSTRACT

The presence of immunosuppressive macrophages that become activated in the tumor microenvironment constitutes a major factor responsible for tumor growth and malignancy. In line with this knowledge, we report here that macrophage proliferation is a significant feature of advanced stages of cancer. Moreover, we have found that a high proportion of proliferating macrophages in human tumors express ERK5. ERK5 was required for supporting the proliferation of macrophages in tumor grafts in mice. Furthermore, myeloid ERK5 deficiency negatively impacted the proliferation of both resident and infiltrated macrophages in metastatic lung nodules. ERK5 maintained the capacity of macrophages to proliferate by suppressing p21 expression to halt their differentiation program. Collectively, these data provide insight into the mechanism underpinning macrophage proliferation to support malignant tumor development, thereby strengthening the value of ERK5-targeted therapies to restore antitumor immunity through the blockade of protumorigenic macrophage activation.

Significance: These findings offer a new rationale for anti-ERK5 therapy to improve cancer patient outcomes by blocking the proliferative activity of tumor macrophages.

Introduction

Tumor-associated macrophages (TAM) are the most abundant cell types across the majority of cancers analyzed (1). Their exquisite ability to shape their phenotype in response to external stimuli allows them to exhibit multifaceted functions in the tumor microenvironments (TME; ref. 2). In particular, as tumors progress, cancer cells produce signals that educate TAMs to secrete a variety of cytokines, growth factors, inflammatory substrates, and proteolytic enzymes involved in cancer progression, malignancy, and resistance to standard-of-care therapeutic interventions (2, 3). Accordingly, TAM abundance has been associated with worse patient prognosis in many, if not all, solid tumors (4, 5). Hence, there has been significant interest in devising macrophage-centered approaches for cancer treatment (2, 3, 6, 7). However, the potential of efficient tailored TAM-directed therapies will only be revealed once the full spectrum of molecular mechanisms governing the programming of protumoral macrophages is discovered.

As a representative example, we have recently analyzed the phenotypic consequences of selective ablation of the ERK5 in the myeloid lineage (8). ERK5 belongs to the family of MAPKs that play key roles in transducing extracellular cues into a wide variety of cellular responses, including changes in gene expression (9). Like other MAPKs, ERK5 is activated upon stimulation by dual phosphorylation of the canonical MAPK activation motif Thr-Glu-Tyr by the MAPK/ERK kinase 5 (MEK5). Nonetheless, ERK5 is very different from the other members of the MAPK family due to a unique extended C-terminal tail (9). The importance of ERK5 in signal transduction is further supported by compelling genetic evidence that the pathway exerts nonredundant functions *in vivo* (10). Notably, we found that ERK5 was required for TAM education by cancer cells (8). Coincidentally, myeloid ERK5 deficiency impaired the growth of 4434 melanoma and Lewis lung adenocarcinoma (LL2) tumor grafts in mice (8). The tumor growth defect caused by the absence of ERK5 correlated with reduced TAM density, in addition to abnormal macrophage polarization (8).

There is compelling evidence that TAM accumulation is a consequence of the constant recruitment of circulating monocytic precursors in the blood, originating from hematopoietic stem cells (HSC) in the bone marrow (11–13). However, other studies revealed that TAMs could also originate from tissue resident macrophages derived from the embryonic yolk sac (14, 15). Furthermore, macrophages in tumor

[1]Department of Biotechnology Chemistry and Pharmacy, University of Siena, Siena, Italy. [2]Division of Cancer Sciences, School of Medical Sciences, Faculty of Biology, Medicine and Health, University of Manchester, Manchester, United Kingdom. [3]Department of Molecular and Translational Medicine, School of Medicine, University of Brescia, Brescia, Italy. [4]Division of Pharmacy and Optometry, School of Health Sciences, Faculty of Biology, Medicine and Health, University of Manchester, Manchester, United Kingdom. [5]School of Medicine, Keel University, Keel, United Kingdom. [6]Department of Medicine-Infectious Diseases, Washington University, Saint Louis, Missouri. [7]Department of Cancer Biology, Dana-Farber Cancer Institute, Boston, Massachusetts. [8]Department of Biological Chemistry and Molecular Pharmacology, Harvard Medical School, Boston, Massachusetts. [9]Department of Pathology and Immunology, Washington University, Saint Louis, Missouri.

Note: Supplementary data for this article are available at Cancer Research Online (http://cancerres.aacrjournals.org/).

Corresponding Authors: Cathy Tournier, University of Manchester, Oxford Road, Manchester M13 9PT, UK. Phone: 44-161-275-5417; Fax: 44-161-275-5082; E-mail: cathy.tournier@manchester.ac.uk; and Emanuele Giurisato, emanuele.giurisato@manchester.ac.uk

Cancer Res 2020;80:3319–30

doi: 10.1158/0008-5472.CAN-19-2416

Published OnlineFirst June 19, 2020; DOI: 10.1158/0008-5472.CAN-19-2416

retain the capacity to proliferate (13, 16–19). This unique feature was shown to markedly contribute to increasing the pool of protumoral TAMs, whether they derive from the yolk sac or the bone marrow, in mammary (13) and pancreatic (20) tumors. Colony-stimulating factor 1 (CSF1, also known as M-CSF) is one of the main factor produced by tumor cells to control the number of TAMs in the TME through stimulation of the CSF1 receptor (21). A previous study showed that CSF1 exerted its mitogenic effect upon binding to the CSF1 receptor and the stimulation of ERK5 in macrophages (22). On the basis of these data, we sought to investigate the impact of ERK5 on TAM proliferation as an important mechanism by which tumor-educated macrophages exhibiting protumoral phenotypes and functions accumulate in the TME.

Materials and Methods

Animal welfare and human samples

Mice were maintained in a pathogen-free facility at the University of Manchester. All animal procedures were performed under license in accordance with the UK Home Office Animals (Scientific Procedures) Act (1986) and approved by the Animal Welfare and Ethical Review Body of the University of Manchester. In particular, mice with tumors were closely monitored by careful clinical examination to allow detection of deterioration of their physical condition. Animals showing signs of distress were sacrificed before any further deterioration in condition occurred. Formalin-fixed paraffin-embedded (FFPE) human tissues obtained with appropriate consents were retrieved from the tissue bank of the Department of Pathology (ASST Spedali Civili di Brescia, Brescia, Italy).

IHC analyses of human tissues

Four-micron-thick sections were double immunostained with antibodies to Ki67 (undiluted; clone 30-9 from Roche) and to CD163 (1:50 dilution; clone 10D6 from Thermo Fisher Scientific). Ki67 was revealed using Novolink Polymer (Leica Biosystems) followed by DAB. After completing the first immune reaction, antibodies to CD163 (1:50 dilution; clone 10D6 from Thermo Fisher Scientific), CD3 (dilution 1:80, clone LN10 from Leica Biosystems), CD20 (dilution 1:250, clone L26 from Leica Biosystems), CD117 (dilution 1:100, polyclonal from Agilent) or CD66b (dilution 1:150, clone G10F5 from Novus Biologicals) were visualized using Mach 4 MR-AP (Biocare Medical), followed by Ferangi Blue (Biocare Medical) as chromogen. For triple IHC, after completing the second immune reactions (Ki67/CD163 or ERK5/CD163), antibody to CD31 (1:30 dilution; clone JC70A from Leica Biosystems) was applied and visualized using Dako REAL Detection System, Alkaline Phoshatase/RED (Agilent). Slides were subsequently counterstained with hematoxylin. Sequentially double immunostaining was performed using a nonpermanent chromogen (AEC) to reveal Ki67. The slides were counterstained with hematoxylin. After digitalization using Aperio Scanscope CS (Leica Mycrosystems), slides were decolored and the Ki67 antibody was stripped using a 2-mercaptoethanol/SDS solution [20 mL 10% (w/v) SDS with 12.5 mL 0.5 mol/L Tris-HCl, pH 6.8, 67.5 mL distilled water and 0.8 mL 2-ME] in a water-bath preheated at 56°C for 30 minutes. Sections were washed for 1 hour in Tris-HCl. Then, after antigen retrieval, anti-ERK5 (1:100 dilution; clone C-20 from Santa Cruz Biotechnology) was applied on the slides and revealed using Novolink polymer followed by DAB. An anti-CD163 was subsequently utilized to localize TAMs (as described above). Slides were newly cover-slipped, digitalized, and then the two digital slides were processed using synchronizing tool of ImageScope. Snapshots of 400× where taken from the two scans and corresponding tissue regions were analyzed using the counter tool. Overlapping of the single images where obtained using Adobe Photoshop.

Mice

Mice were identified by PCR on genomic DNA, as described previously (8). For melanoma grafts, 4434 melanoma cells were subcutaneously transplanted in the flanks of 8 to 12 weeks old syngeneic C57Bl/6 mice (8). For lung experimental metastasis, 2×10^5 B16F10 melanoma cells resuspended in 0.1 mL PBS were injected via the lateral tail vein using a 27-gauge needle. Mice were killed between 15 and 20 days after injection and tissues were isolated and fixed in 10% neutral-buffered formalin, prior to being processed for immunofluorescence analysis as described previously (8). Sections were counterstained with hematoxylin and eosin (H&E) and surface metastatic foci in lung left lobes were counted under a dissecting microscope. For quantitation of metastatic nodule size, photos of random fields were obtained (using low-magnitude 4× and 10× lens), and then the sizes of at least 20 nodules were determined using NIH Image software (version 1.44) and averaged.

Flow cytometry

Mononuclear single-cell suspensions from mouse tumors, lungs, and spleen were obtained as indicated in the Supplementary Data available with this article online (Supplementary Materials and Methods) and analyzed by FACS, as described previously (8). Antibodies utilized for flow cytometry analysis and magnetic bead purification are provided in the Supplementary Materials and Methods. For determining cell proliferation, primary bone-derived macrophages were pulse labeled *in vitro* with 100 μmol/L 5-bromo-2′-deoxyuridine (BrdUrd; Sigma) for 30 minutes at 37°C. Cells were subsequently harvested, fixed in 4% formaldehyde for 15 minutes at room temperature, and permeabilized by incubation in ice-cold methanol for 30 minutes. Cells were washed in PBS and incubated with a primary antibody to BrdUrd (1:200 dilution; CST#5292) for 60 minutes, followed by incubation with a secondary Alexa Fluor 488-conjugated anti-mouse IgG F(ab')2 fragment (1:100 dilution; CST#4408) for 30 minutes at room temperature.

Immunoblot analysis of bone marrow–derived macrophages

Primary murine macrophages were obtained from bone marrow cells isolated from femurs of wild-type (WT) or genetically modified mice and polarized by exposure to tumor cell-conditioned media (1/2 dilution), as described previously (8). $erk5^{F/F}$ and $CMV\text{-}Cre^{ER}$; $erk5^{F/F}$ macrophages incubated with 4-hydroxytamoxifen (4-HT, 0.1 μmol/L) were referred to as $erk5^{wt}$ and $erk5^{\Delta/\Delta}$, respectively. Proteins (30 μg) were subsequently extracted in RIPA buffer, resolved by SDS-PAGE and transferred to an Immobilon-P membrane (Millipore, Inc.). The membranes were saturated in 3% nonfat dry milk and probed overnight at 4°C with antibodies to ERK5 (1:1,000 dilution; CST3372), p21 (1:1,000 dilution; CST2947), or tubulin (1:1,000 dilution; CST2125). Immuno-complexes were detected by enhanced chemiluminescence with immunoglobulin G coupled to horseradish peroxidase as the secondary antibody (GE Healthcare).

Quantitative real-time PCR

Total RNA was reversed transcribed and quantified by RT-PCR using the SYBR Green I Core Kit (Eurogentec), as described

Published OnlineFirst June 19, 2020; DOI: 10.1158/0008-5472.CAN-19-2416

previously (8). Sequences of the forward and reverse primers are indicated in the Supplementary Data available with this article online (Supplementary Table S1). Results were analyzed using the $2^{-\Delta\Delta G}$ method. The level of expression of mRNA was normalized to *Gapdh* and *Pgk1* mRNA.

Statistical analysis

All *P* values were generated using an unpaired Student *t* test and one-way ANOVA with Tukey's correction for multiple comparisons. Data were analyzed using Prism software (GraphPad). For all tissue experiments, images are representative of cohorts of at least 3 mice.

Data availability

The authors declare that all data supporting the findings of this study are available within the article and its supplementary information files or from the corresponding authors on reasonable request.

Results

Human neoplastic tissues comprise high numbers of proliferative macrophages

To demonstrate that proliferating TAMs were characteristic of human cancer, we initially screened a large set of human primary malignant lesions ($n = 197$) using tissue microarrays. Representative images show the noticeable increase in the number of proliferating macrophages ($Ki67^+CD163^+$ cells) in squamous cell carcinoma (SCC), lung adenocarcinoma, and breast carcinoma compared with normal tissues (**Fig. 1A–I**). This was confirmed by quantitative analysis of $Ki67^+$ TAMs (**Fig. 1J–L**). The number of $Ki67^+CD163^+$, as well as the total number of macrophages are included in Supplementary Table S2A. Likewise, a high number of proliferating TAMs was detected in primary human hepatocarcinoma, colon, ovary, bladder carcinoma, melanoma, mesothelioma, and metastatic melanoma and carcinoma (Supplementary Fig. S1). To explore the possibility that macrophage accumulation through proliferation was a significant feature of malignancy, we compared

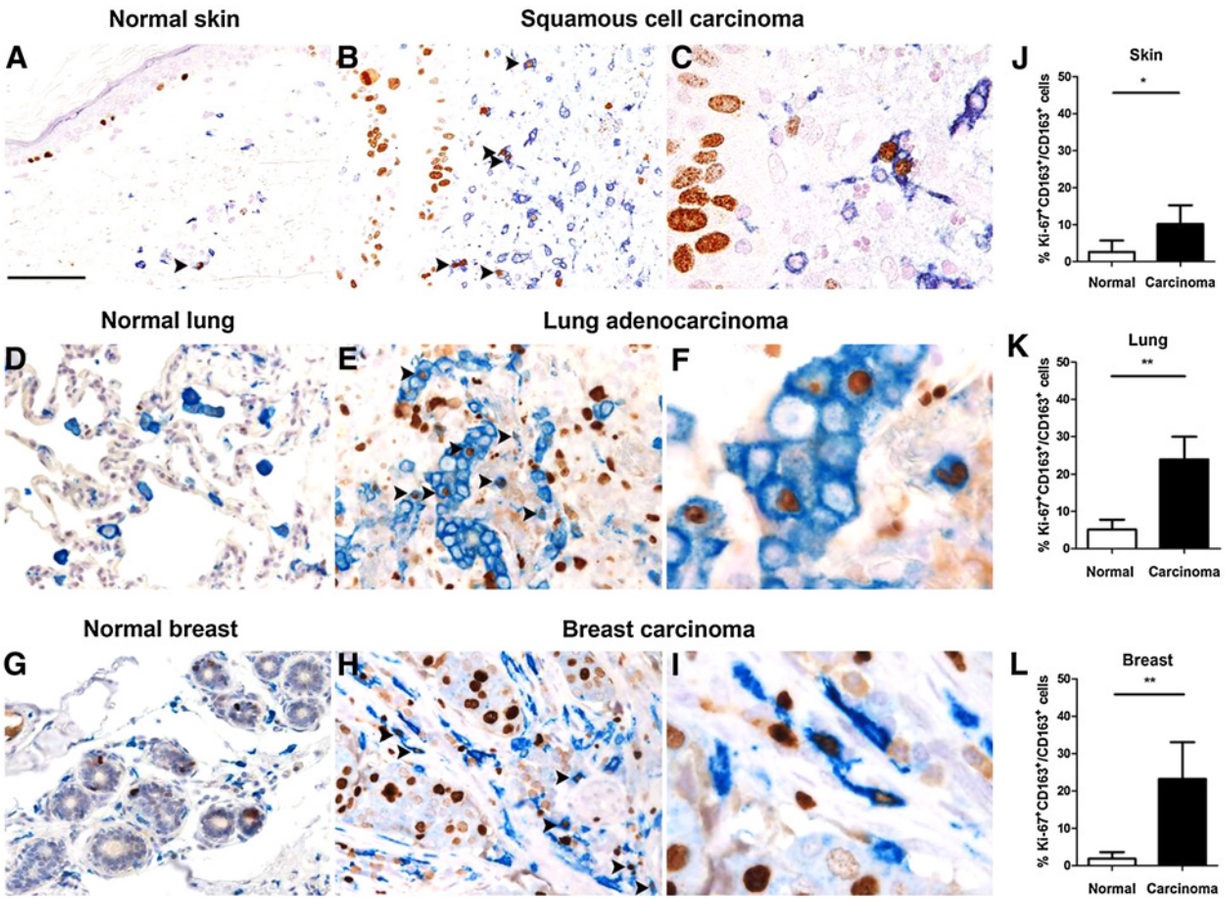

Figure 1.

Human tumors contain a high number of proliferating macrophages. Sections from normal and neoplastic tissues, including skin (**A–C**), lung (**D–F**), and breast (**G–I**), were double stained for Ki67 (brown) and CD163 (blue). Original magnification, ×200; scale bar, 100 μm (**A**, **B**, **D**, **E**, **G**, and **H**) and ×600; scale bar, 33 μm (**C**, **F**, and **I**). Arrows in ×200, proliferating macrophages. For quantitative analysis, double-positive cells ($Ki67^+CD163^+$) were counted (at least 100 macrophages/case) in normal skin ($n = 5$), cutaneous squamous cell carcinoma ($n = 11$), normal lung ($n = 4$), lung adenocarcinoma ($n = 10$), normal breast ($n = 4$), and breast carcinoma ($n = 12$). The data presented as percentage of proliferating macrophages (**J–L**) correspond to the mean ± SD. *, $P < 0.05$; **, $P < 0.01$ compares normal versus tumor tissues.

Published OnlineFirst June 19, 2020; DOI: 10.1158/0008-5472.CAN-19-2416

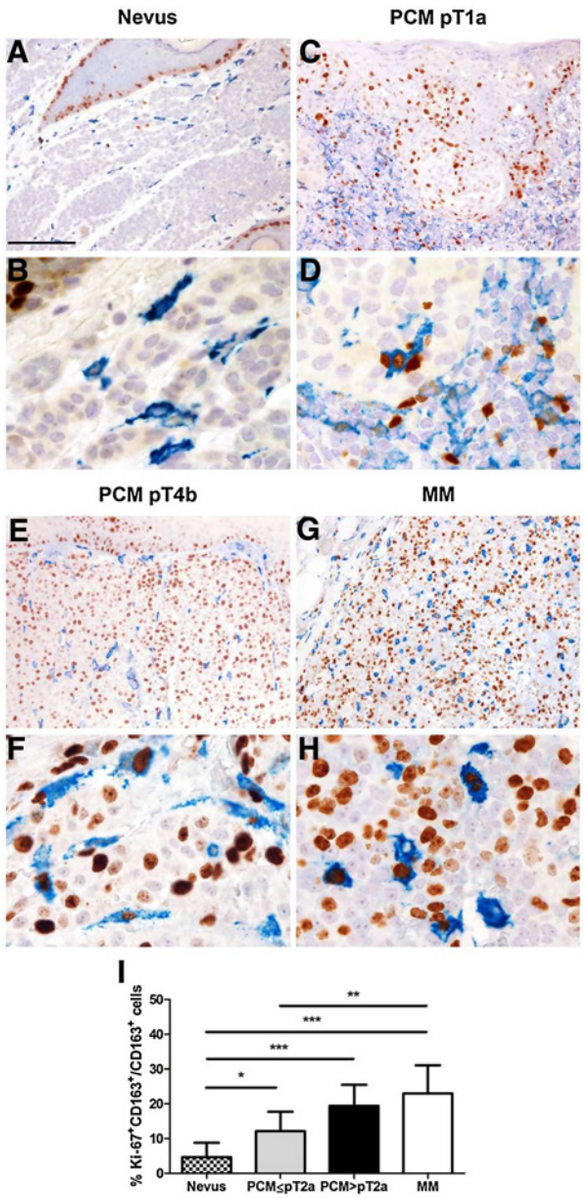

Figure 2.

Proliferating TAMs in primary and metastatic melanomas. Sections from benign nevus (**A** and **B**), PCM (**C–F**) at different pathologic stages, and dermal metastasis of cutaneous melanoma (MM; **G** and **H**) were double stained for Ki67 (brown) and CD163 (blue). Original magnification, ×100; scale bar, 200 μm (**A**, **C**, **E**, and **G**) and ×400; scale bar, 50 μm (**B**, **D**, **F**, and **H**). **I,** The clinical significance of TAM proliferation in melanocytic lesions was tested by counting the number of double-positive cells ($Ki67^+CD163^+$) in benign nevi ($n = 10$), PCM ($n = 20$), and MM ($n = 10$). The data presented as percentages of proliferating macrophages in the four pathologic groups correspond to the mean ± SD. *, $P < 0.05$; **, $P < 0.01$; ***, $P < 0.001$ compares between distinct pathologic stages.

the number of $Ki67^+CD163^+$ macrophages in human melanoma at different stages of tumor progression. These included benign nevus (**Fig. 2A** and **B**), early (pT1a) and late (pT4b) stage primary cutaneous melanoma (PCM; **Fig. 2C–F**), and dermal metastasis of cutaneous melanoma (MM; **Fig. 2G** and **H**). Remarkably, we observed that the percentage of proliferating TAMs significantly increased as the disease progressed (**Fig. 2I**; Supplementary Table S2A). In contrast, no marked difference was observed between benign nevus and normal skin tissues. Together, these observations clearly indicated that local macrophage proliferation was a common hallmark of human tumors and a potentially important prognostic marker of malignancy.

Tumor macrophage proliferation is dependent on ERK5

We had previously found that macrophage density was markedly reduced in carcinoma grafts derived from myeloid ERK5 deficient mice compared with controls (8). Utilizing a similar approach based on our *LysM-Cre;erk5$^{F/F}$* model, we confirmed that the number of TAMs in melanoma grafts decreased by almost two-fold in the absence of ERK5 (Supplementary Figs. S2A and S2B). Accordingly, the percentage of $Gr1^-F4/80^+$ macrophages expressing CD206 was reduced in melanoma grafts derived from *LysMCre;erk5$^{F/F}$* mice compared with that from *erk5$^{F/F}$* (Supplementary Figs. S2C–S2E). Importantly, the reduction in macrophage density caused by myeloid ERK5 deficiency coincided with reduced melanoma cell proliferation in the tumor (Supplementary Fig. S3).

On the basis of these data, we examined a possible association between ERK5 expression and tumor macrophage proliferation in human cancer. This was achieved by employing Aperio Scanscope digitalization to sequentially detect Ki67 (AEC) and ERK5 (brown) in $CD163^+$ (blue) cells in human tumor sections. Between 60% and 50% of proliferating TAMs in lung metastasis of cutaneous melanoma and ovarian carcinoma expressed ERK5 in the nucleus (**Fig. 3A–F**). Likewise, nuclear ERK5 was detected in around 90% and 40% of $Ki67^+CD163^+$ macrophages present in cell blocks of pleural effusion of lung adenocarcinoma (**Fig. 3G–I**) and cytospin preparation of peritoneal wash of ovarian carcinoma (**Fig. 3J–L**), respectively. Proliferating $ERK5^+$ macrophages were found in both intratumoral area (cutaneous melanoma) and intratumoral stroma (second raw ovarian carcinoma). Further analyses of breast carcinoma also demonstrated the presence of $Ki67^+ERK5^+$ macrophages in peritumoral area, close to tumor vessel at the invasion edge (Supplementary Fig. S4). On the basis of these observations, we concluded that human tumors comprised a high proportion of proliferating TAMs expressing ERK5 scattered around the tissue. Unlike TAMs, $CD117^+$ mast cells and $CD66b^+$ neutrophils exhibited a predominantly cytoplasmic ERK5 staining, indicative of a low level of ERK5 activity in these cells (Supplementary Fig. S5). Moreover, the number of ERK5-expressing $CD3^+$ T and $CD20^+$ B cells was very low, suggesting that ERK5 might not play a critical role in the adaptive immune system of the TME (Supplementary Fig. S5).

To establish whether ERK5 was required for mediating tumor macrophage proliferation, we sought to analyze the impact of myeloid ERK5 deficiency in excised murine melanoma and carcinoma grafts. Tumor sections were processed by immunofluorescence staining with antibodies to Ki67 and to Iba1, a commonly used cell surface marker to label total TAMs. The results showed around 50% reduction in the proportion of proliferating $Ki67^+Iba1^+$ macrophages in tumors derived from *LysM-Cre;erk5$^{F/F}$* mice compared with *erk5$^{F/F}$* controls (**Fig. 4A** and **B**; Supplementary Figs. S6A and S6B; Supplementary Table S2B). Moreover, ERK5-deficient macrophages purified from melanoma or carcinoma grafts expressed a lower level of positive regulators of cell proliferation, for example, *Ets2, Ki67*, and *c-Jun* transcripts, compared with WT cells (**Fig. 4C**; Supplementary Fig. S6C). Conversely, carcinoma macrophages lacking ERK5 exhibited increased mRNA expression of two important transcription

Published OnlineFirst June 19, 2020; DOI: 10.1158/0008-5472.CAN-19-2416

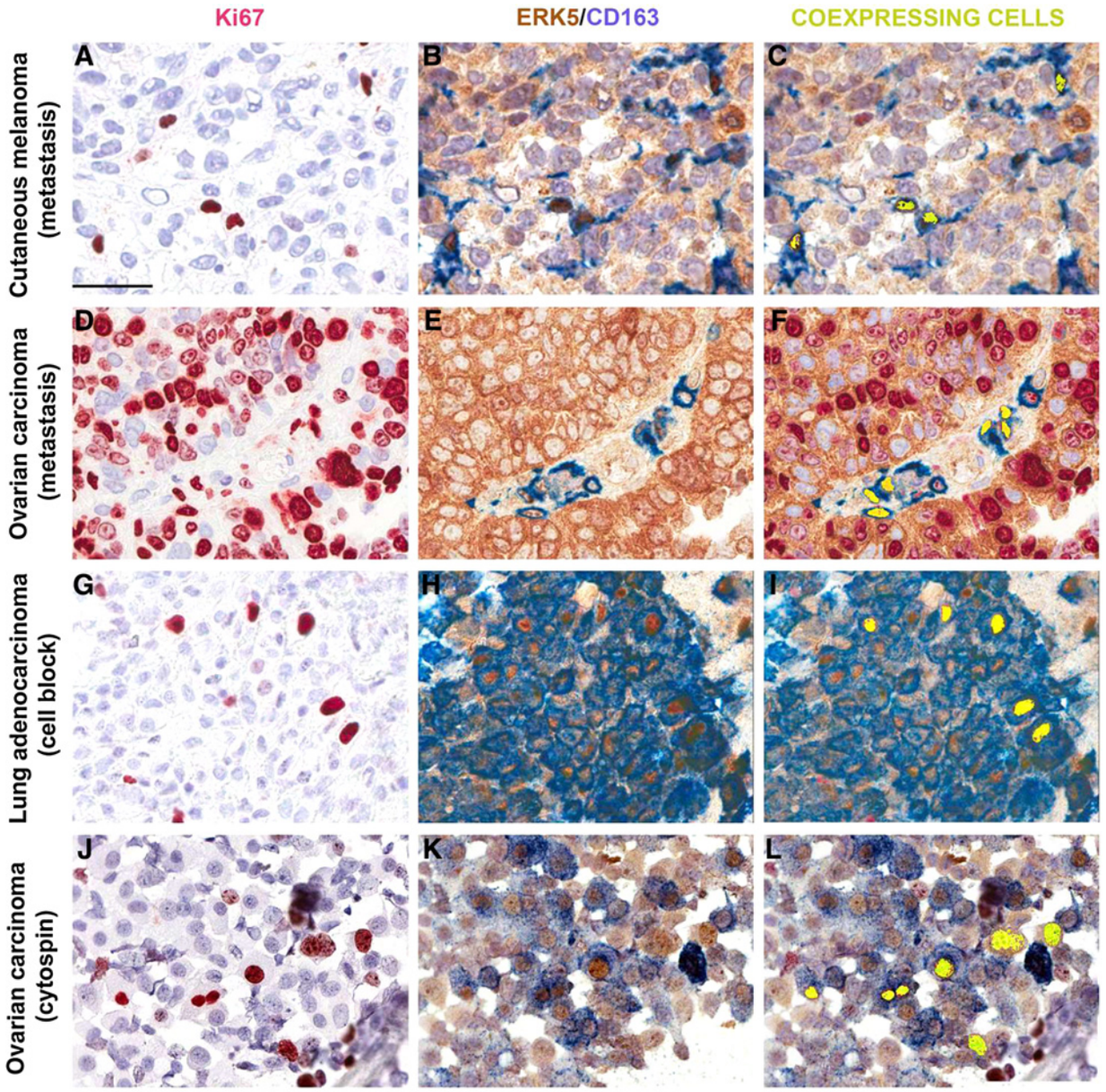

Figure 3.

Human proliferating TAMs express ERK5. Ki67, and ERK5 colocalization in TAMs was demonstrated by double sequential immunostaining in two bioptical [a lung metastasis of cutaneous melanoma (**A–C**) and a vaginal localization of ovarian carcinoma (**D–F**)] and two cytological [a cell block of pleural effusion of lung adenocarcinoma (**G–H**) and a cytospin preparation of peritoneal wash of ovarian carcinoma (**J–L**)] samples. Slides were re-digitalized and images were taken using synchronizing and snapshot tools (×400). False color images (**C**, **F**, **I**, and **L**) show overlapping of Ki67, ERK5, and CD163 staining. Yellow, $CD163^{+}$ TAMs coexpressing Ki67 and ERK5.

factors associated with macrophage differentiation, namely *c-Maf* and *MafB* (Supplementary Fig. S6C). A similar increase in *c-Maf* level was detected in purified ERK5-deficient macrophages from melanoma, although no significant difference was observed in *MafB* expression (**Fig. 4C**). In addition, the cyclin-dependent protein kinase inhibitor *p21* was significantly upregulated in the absence of ERK5 (**Fig. 4C**; Supplementary Fig. S6C). We confirmed by immunoblot analysis that p21 protein level was noticeably increased in *LysM-Cre;erk5*$^{F/F}$ macrophages polarized *in vitro* by incubation with melanoma 4434 cell-conditioned medium (Supplementary Fig. S7A). This coincided with increased p53 expression and decreased level of pSTAT3(Tyr705) and cyclin D1. In contrast, the absence of ERK5 did not affect ERK1/2 (Supplementary Fig. S7A).

ERK5 is a key suppressor of p21 expression during the maturation and differentiation of monocytes into macrophages

To provide direct evidence that ERK5 was a positive regulator of TAM proliferation, we prepared genetically modified macrophages

Published OnlineFirst June 19, 2020; DOI: 10.1158/0008-5472.CAN-19-2416

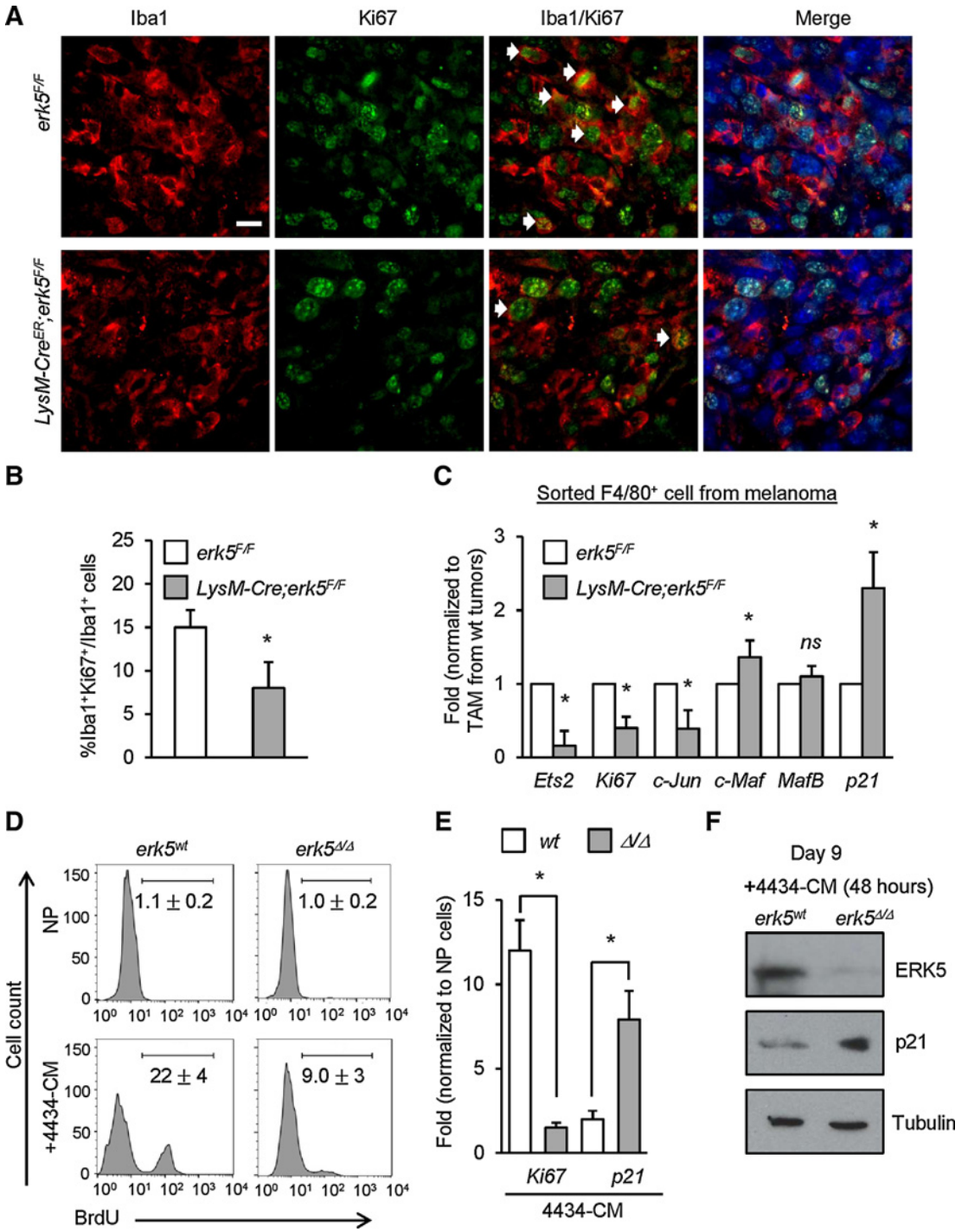

Figure 4.

Myeloid ERK5 is required for TAM proliferation. **A,** Immunofluorescence imaging of melanoma grafts sections stained for Iba1 (red) and Ki67 (green). DNA was stained with DAPI (blue). Scale bar, 15 μm. **B** and **C,** Quantification (**B**) of proliferating (Ki67$^+$) macrophages (Iba1$^+$) in tumor grafts with ImageJ and qRT-PCR analysis (**C**) of positive (*Ets2, Ki-67, c-Jun*) and negative (*c-Maf, MafB* and *p21*) cell-cycle regulators in Gr1$^-$/F4/80$^+$ sorted macrophages from 4434 melanoma tumor grafts derived from *erk5*$^{F/F}$ and *LysM-Cre;erk5*$^{F/F}$ mice. The data correspond to the mean ± SD ($n = 3$ tumors per genotype). *, $P < 0.05$ compares tumor grafts from *erk5*$^{F/F}$ and *LysM-Cre;erk5*$^{F/F}$ mice. *ns*, no significant difference. **D** and **E,** Histograms represent quantitative analysis of BrdUrd$^+$ macrophages (**D**) and qRT-PCR analysis of *Ki-67* and *p21* expression in NP and 4434 polarized *erk5*^{wt} and *erk5*$^{\Delta/\Delta}$ macrophages (**E**). The data correspond to the mean ± SD of three independent experiments performed in triplicate. *, $P < 0.05$ compares *erk5*^{wt} and *erk5*$^{\Delta/\Delta}$ macrophages. **F,** Immunoblot analysis of ERK5 and p21 expression in *erk5*^{wt} and *erk5*$^{\Delta/\Delta}$ macrophages cultured for 9 days *in vitro* prior to being exposed to 4434-CM for 48 hours. Tubulin expression was used as loading control.

Published OnlineFirst June 19, 2020; DOI: 10.1158/0008-5472.CAN-19-2416

from the bone marrow of *CMV-Cre^{ER};erk5$^{F/F}$* mice to permit inducible *erk5* deletion *in vitro* by incubation with 4-HT (Supplementary Fig. S7B). Initially, we confirmed by short-term BrdUrd incorporation that nonpolarized (NP) macrophages in steady state were mostly quiescent, whereas more than 20% of macrophages polarized by incubation with 4434 melanoma cell-conditioned media (4434-CM) were actively replicating their DNA (**Fig. 4D**). Increased tumor macrophage proliferation was clearly reduced in the absence of ERK5 (**Fig. 4D**). Accordingly, polarized *erk5*$^{\Delta/\Delta}$ macrophages exhibited a much lower level of *Ki67* transcript compared with WT cells (**Fig. 4E**). This correlated with a significant upregulation of p21 at mRNA and protein level (**Fig. 4E** and **F**). These results led us to conclude that ERK5 was required for mediating the mitogenic response of macrophages to tumor soluble factors, at least in part, via suppressing p21 expression.

We and others had previously observed that functional disruption of ERK5 signaling advanced macrophage differentiation *in vitro* (8, 23). Therefore, we tested whether the mitogenic effect of ERK5 was a consequence of its ability to suppress differentiation. Consistent with our previous data, ERK5 ablation in bone marrow cells impaired the ability of maturing macrophages to proliferate (**Fig. 5A**; Supplementary Figs. S7C and S7D). Moreover, the absence of ERK5 significantly accelerated the kinetic of monocyte differentiation *in vitro* (**Fig. 5B** and **C**). Notably, the intensity of F4/80 and CD115 staining was distinctively higher in *erk5*$^{\Delta/\Delta}$ compared with *erk5*^{wt} maturing macrophages at day 3, indicative of a more advanced macrophage differentiation in the absence of ERK5 (**Fig. 5C** and **D**). Interestingly, the differentiation of *erk5*$^{\Delta/\Delta}$ monocytes was associated with a strong upregulation of p21 expression (**Fig. 5E**). Given that p21 is crucial for the maturation and differentiation of macrophages (24, 25), we proposed that the downregulation of p21 expression by ERK5 constituted one potentially important mechanism that maintains macrophages in a phenotypic state capable of responding to mitogenic factors produced by cancer cells (**Fig. 5F**).

Inhibition of ERK5 activity blocks tumor macrophage proliferation

The detection of an electrophoretic migratory shift characteristic of ERK5 phosphorylation provided evidence that ERK5 was activated in macrophages stimulated with 4434-CM or B16F10-CM (Supplementary Fig. S8A). Accordingly, preincubation with the JWG-045 compound caused the disappearance of the slow migrating band as a consequence of inhibition of ERK5 activity and the loss of C terminal tail autophosphorylation (Supplementary Fig. S8A). In contrast, JWG-045 did not affect ERK1/2 phosphorylation. Similar to the loss of ERK5 protein expression, inhibition of ERK5 by JWG-045 reduced by half the number of proliferating tumor macrophages (Supplementary Figs. S8B and S8C). However, given that the first generation of pharmacologic ERK5 inhibitors exhibited nonspecific effect on BRD4 proteins (26), we wanted to insure that ERK5 activation was essential for promoting the proliferation of TAMs by other means. Therefore, *erk5*$^{\Delta/\Delta}$ macrophages were coinfected with adenoviruses encoding Ha-tagged constitutive active (ca) MEK5 and flag-tagged (F) WT or dominant negative mutant (AEF) ERK5 (Supplementary Fig. S9A). As expected, ERK5(AEF) did not display the mobility retardation shift characteristic of ERK5(WT) phosphorylation by caMEK5 (Supplementary Fig. S9B). Moreover, unlike ERK5(WT), ERK5(AEF) expressed together with caMEK5 significantly reduced the number of proliferating macrophages exposed to 4434-CM (Supplementary Figs. S9C and S9D). Collectively, these data demonstrated that ERK5 activation by MEK5 was critical for tumor-induced macrophage proliferation.

ERK5-mediated macrophage proliferation supports melanoma tumor metastasis *in vivo*

Given the correlation between TAM proliferation and melanoma invasiveness in human (**Fig. 2**), we sought to investigate the impact of myeloid ERK5 deficiency in metastasis. Melanoma B16F10 cells were transplanted intravenously via the tail vein in *erk5*$^{F/F}$ and *LysM-Cre;erk5*$^{F/F}$ mice. Animals were sacrificed after 2 to 3 weeks and postmortem analyses showed that the lungs of *LysM-Cre;erk5*$^{F/F}$ mice exhibited less metastases compared with control *erk5*$^{F/F}$ animals (**Fig. 6A**). Quantitative analysis indicated that the number of metastatic lung nodules was reduced by half in myeloid ERK5-deficient mice (**Fig. 6B**). To further characterize the metastasis lowering associated with myeloid ERK5 ablation, lung sections of *erk5*$^{F/F}$ and *LysM-Cre;erk5*$^{F/F}$ transplanted mice were processed by H&E staining. Metastatic foci in both groups were distributed as perivascular and subpleural lesions (**Fig. 6C**). However, consistent with our previous macroscopic observation, their number and size were significantly lower in the absence of ERK5 (**Fig. 6C** and **D**). Immunofluorescence analysis of lung tissue sections with an antibody to Iba1 confirmed that ERK5 ablation significantly reduced TAM density in melanoma metastases (Supplementary Fig. S10). Accordingly, lungs of B16F10-bearing *LysM-Cre;erk5*$^{F/F}$ animals exhibited a much lower percentage of Gr1^{-}F4/80^{+} macrophages (**Fig. 6E** and **F**). We also noted that, although there was no difference in the number of Gr1^{+}F4/80^{-} neutrophils, the percentage of Gr1^{+}F4/80^{+} monocytes was significantly lower in *LysM-Cre;erk5*$^{F/F}$ than in *erk5*$^{F/F}$ lung samples (**Fig. 6F**). This coincided with a lower number of circulating *LysM-Cre;erk5*$^{F/F}$ CD11b+F4/80^{+} monocytes (Supplementary Fig. S11A). Accordingly, myeloid ERK5 deficiency significantly reduced the percentage of monocytes proliferating in the blood or in the bone marrow of B16F10 transplanted animals (Supplementary Figs. S11B and S11C).

Lung macrophages from *erk5*$^{F/F}$ and *LysM-Cre;erk5*$^{F/F}$ naïve and B16F10-bearing mice were subsequently analyzed by flow cytometry to distinguish interstitial (infiltrating) from alveolar (resident) macrophages based on different level of expression of CD11b and Cd11c markers (27, 28). CD64 was utilized as an alternate marker to F4/80 to distinguish macrophages from dendritic cells. As expected, normal lungs were devoided of CD11b^{+}CD64^{+} interstitial macrophages (Supplementary Figs. S12A and S12B). Moreover, the small percentage of CD11c^{+}CD64^{+} alveolar macrophages was unaffected by the absence of ERK5 (Supplementary Figs. S12C and S12D). In contrast, the absence of ERK5 reduced the percentage of both interstitial (CD11c$^{low/-}$F4/80^{+}) and alveolar (CD11c^{+}F4/80^{+}) macrophages in metastatic lung nodules (**Fig. 7A** and **B**). F4/80^{+} cells were subsequently purified by magnetic-assisted cell sorting, and CD11b^{+} and CD11c^{+} macrophages were analyzed separately by flow cytometry for Ki67 expression (Supplementary Fig. S13A). We confirmed that F4/80^{+} sorted cells were positive for CD64 expression (Supplementary Figs. S13B and S13C). Importantly, we found that myeloid ERK5 deficiency decreased the number of proliferating metastatic lung interstitial (**Fig. 7C** and **D**) and alveolar (**Fig. 7E** and **F**) macrophages. Together, these findings provided a further compelling demonstration that ERK5-mediated macrophage proliferation was an integral component of tumor malignancy.

Discussion

Targeted therapies aimed at depleting macrophages in the TME have been actively pursued to combat various cancers (2, 3, 6, 7). One of the most advance approaches rely on the blockade of CSF1/CSF1 receptor, given that CSF1 is highly expressed in several types of human

Published OnlineFirst June 19, 2020; DOI: 10.1158/0008-5472.CAN-19-2416

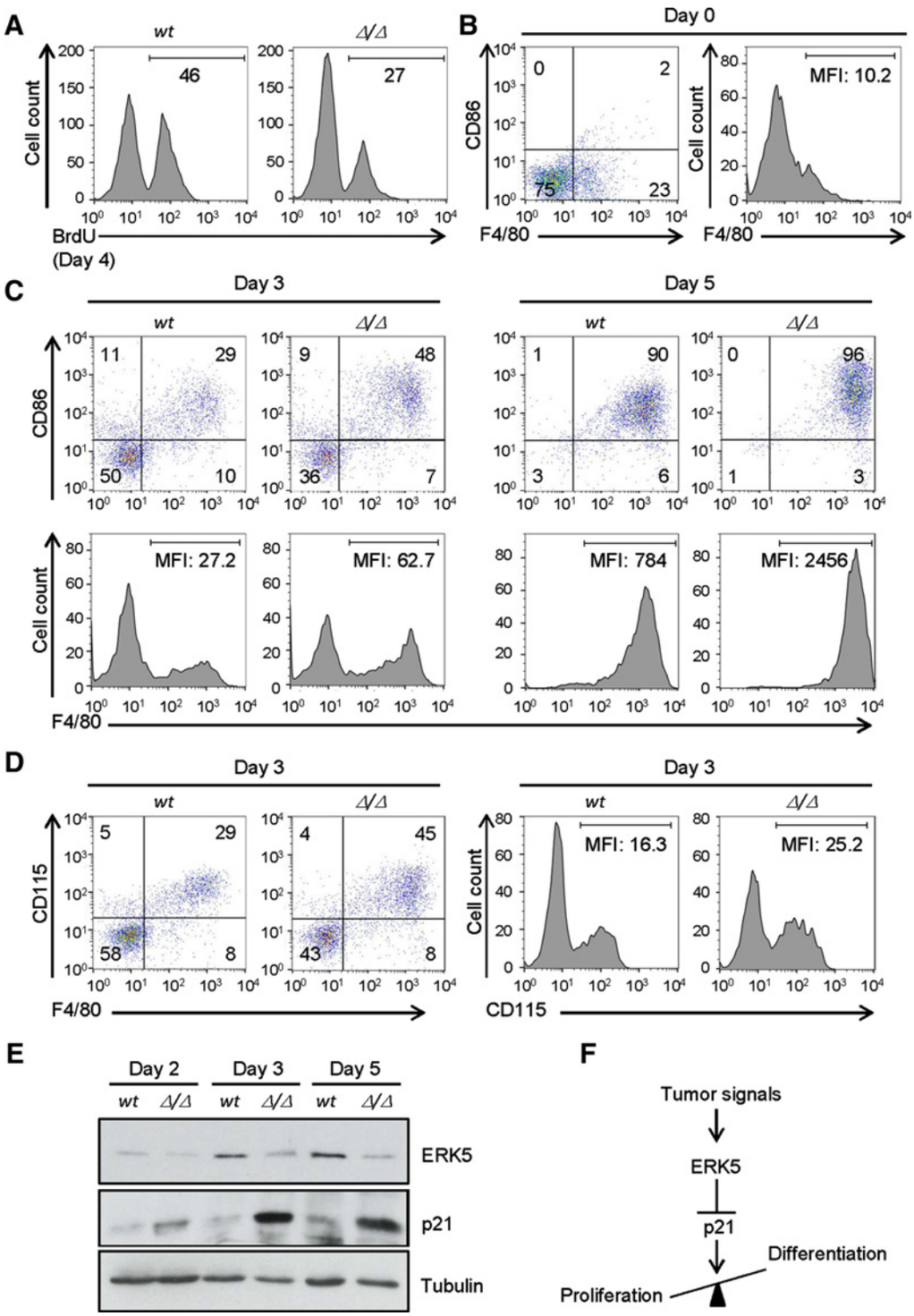

Figure 5.

ERK5 suppresses macrophage differentiation through negative regulation of p21. **A,** Flow cytometry analysis of BrdUrd incorporation in macrophages derived from the maturation of *erk5*^{wt} and *erk5*$^{\Delta/\Delta}$ monocytes. The percentage of BrdUrd^{+} cells is indicated in the plot. **B–D,** Flow cytometry analysis and quantification of F4/80^{+}CD86^{+} (**B** and **C**) and F4/80^{+}CD115^{+} (**D**) cells during the maturation (days 0, 3, and 5) of *erk5*^{wt} and *erk5*$^{\Delta/\Delta}$ monocytes/macrophages. The level of expression of F4/80 and CD115 (MFI) is indicated in each histogram plot. Data are representative of at least two independent experiments. **E,** Immunoblot analyses show that ablation of ERK5 in monocytes/macrophages correlate with increased p21 expression. Tubulin expression was used as loading control. Similar results were obtained in two independent experiments. **F,** Schematic model illustrating how ERK5 blocks macrophage differentiation by suppressing p21 expression.

Published OnlineFirst June 19, 2020; DOI: 10.1158/0008-5472.CAN-19-2416

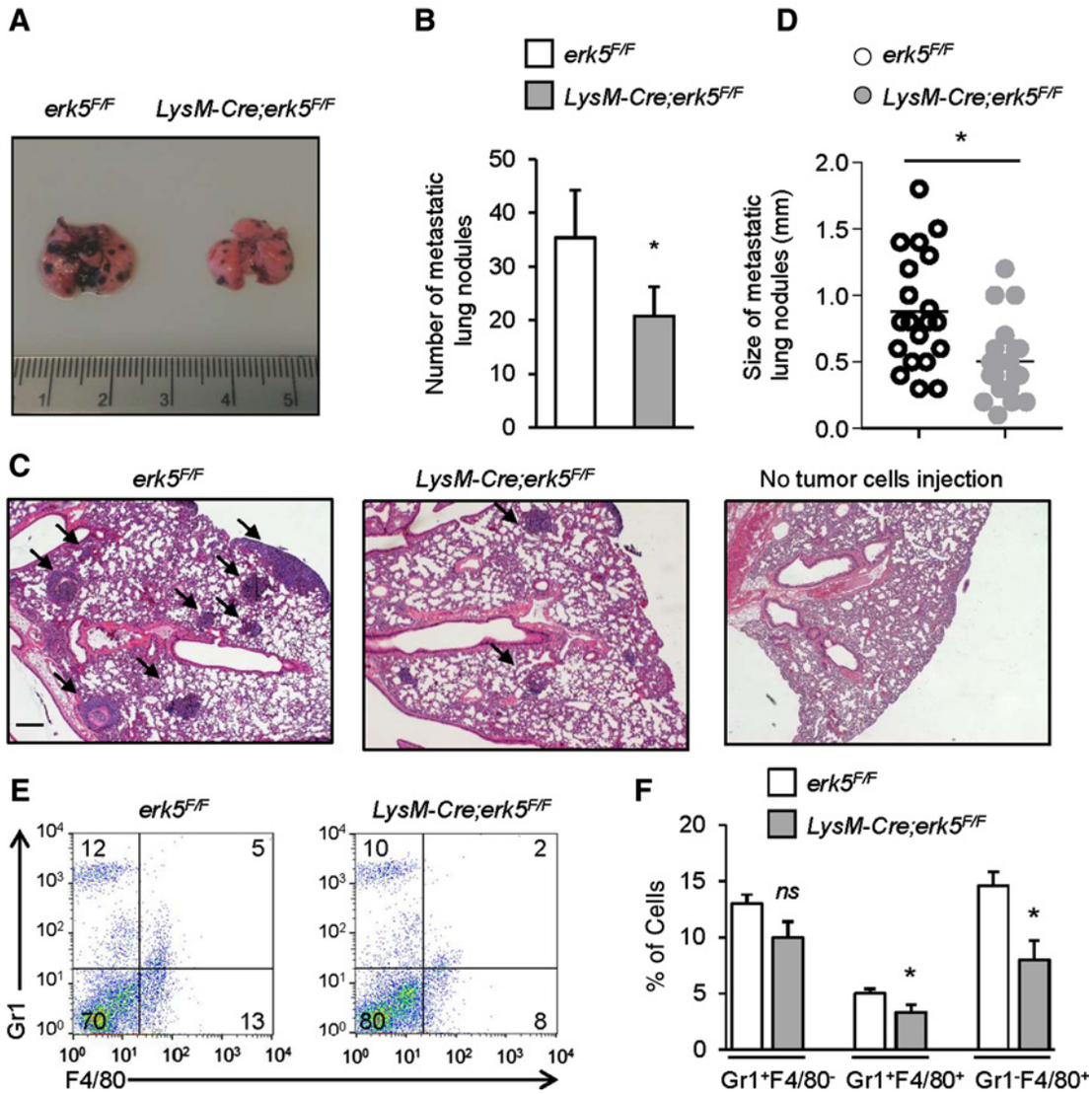

Figure 6.

Myeloid ERK5 supports melanoma tumor metastasis *in vivo*. **A,** Representative pictures of lungs bearing metastases 18 days after intravenous transplantation of B16F10 melanoma cells in the tail vein of *erk5*$^{F/F}$ and *LysM-Cre;erk5*$^{F/F}$ mice. **B,** Quantification of the number of metastatic lung nodules in mice. *, $P < 0.01$ indicates a significant difference between *erk5*$^{F/F}$ *and LysM-Cre;erk5*$^{F/F}$ ($n = 10$ animals per genotype). **C,** Representative H&E sections of lungs from *erk5*$^{F/F}$ and *LysM-Cre;erk5*$^{F/F}$ mice, 18 days after transplantation of melanoma cells. Arrows, metastatic foci. Scale bar, 200 µm. **D,** Size distributions of B16F10 metastatic foci. *, $P < 0.01$ indicates a significant difference between *erk5*$^{F/F}$ *and LysM-Cre;erk5*$^{F/F}$ ($n = 14$ animals per genotype). **E,** Representative flow cytometry analysis and quantification of live (DAPI$^-$) myeloid cell populations in the lung, 18 days after transplantation of melanoma cells. **F,** Graphical analysis of **E** showing a specific reduction in the percentage of Gr1$^-$F4/80$^+$ macrophages in lungs from *LysM-Cre;erk5*$^{F/F}$ animals bearing melanoma metastases. The data correspond to the mean ± SD ($n = 3$ animals per genotype). *, $P < 0.05$ compares *erk5*$^{F/F}$ and *LysM-Cre;erk5*$^{F/F}$ mice. *ns*, no significant difference.

tumors with poor patient outcomes and the dominant role of this signaling pathway in fostering the development of various populations of macrophages exhibiting protumor properties (29, 30). In particular, in mammary cancer, CSF1 produced by tumor cells was shown to drive the accumulation of TAMs that supply the neoplasm with the crucial EGF (31). This was consistent with an earlier study, which demonstrated that the genetic loss of *csf1* significantly reduced metastasis in mammary tumors (32). Importantly, although less effective, neutralizing CSF1 in breast cancer xenografts decreased tumor growth (33). Further studies confirmed that depleting TAMs by CSF1R signaling blockade delayed tumor progression and reduced metastasis, but also enhanced the efficacy of several other standard therapies in various murine models of solid tumors (30).

However, despite these promising results, clinical trials have brought modest clinical benefits for patients with cancer, emphasizing the necessity for far more in depth understanding of the mechanisms underpinning the accumulation of protumoral macrophage populations in preclinical settings. In particular, despite being differentiated, macrophages preserve a certain capacity to self-renew in response to various environmental cues (34). This is significant given that subsets

Published OnlineFirst June 19, 2020; DOI: 10.1158/0008-5472.CAN-19-2416

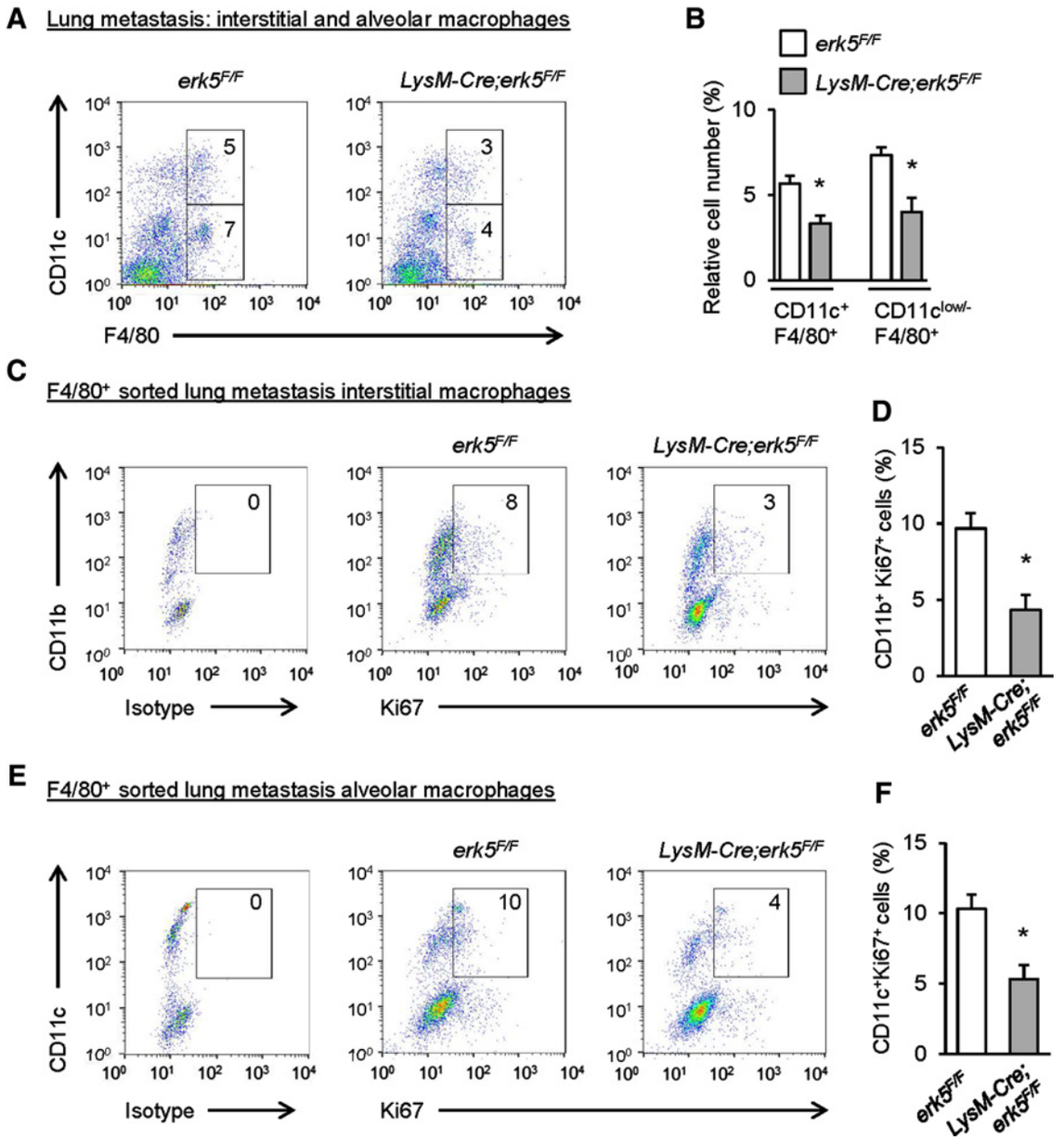

Figure 7.

ERK5 deficiency blocks alveolar and interstitial macrophage proliferation in melanoma lung metastasis. **A,** Representative flow diagram and quantification of $CD11c^+F4/80^+$ (alveolar) and $CD11c^{low/-}F4/80^+$ (interstitial) macrophages in the lung of mice 18 days after transplantation of B16F10 melanoma cells. **B,** Graphical analysis of **A** showing a reduced percentage of alveolar and interstitial macrophages in the lungs of *LysM-Cre;erk5$^{F/F}$* mice. The data correspond to the mean ± SD ($n = 3$ tumors). **C–F,** $F4/80^+$ sorted macrophages from **A** were separately analyzed for the expression of CD11b, CD11c, and Ki67. Representative plots and quantification of proliferating $F4/80^+$ interstitial ($CD11b^+Ki67^+$; **C** and **D**) and alveolar ($CD11c^+Ki67^+$; **E** and **F**) macrophages are shown. The data correspond to the mean ± SD ($n = 3$ tumors). *, $P < 0.05$ compares *erk5$^{F/F}$* and *LysM-Cre;erk5$^{F/F}$* mice.

of TAMs were observed to proliferate in sarcomas (17), breast carcinomas (13, 18, 19), and pancreatic cancer (20). Furthermore, there is a possibility that increased macrophage proliferation following the cessation of TAM depletion contributes to accelerating tumor growth in a murine model of breast cancer metastasis (35). Our demonstration that macrophage proliferation was a common feature of cancer patients across various malignant tumor types added further weight to the idea that pools of macrophages can expand through local self-renewal in tumor tissue. Consistent with evidence that TAM density positively correlates with the malignant progression of most solid tumors (2–5), including melanoma (36, 37), decreased TAM proliferation caused by myeloid ERK5 ablation halted the growth of murine melanoma graft (8) and the capacity of melanoma cells to form lung metastasis.

On the basis of previous analyses of ERK5 in cancer cells, ERK5 activity may promote macrophage proliferation by suppressing p53-

mediated transcriptional upregulation of p21 through blocking PML-dependent sequestration of MDM2 in cancer cells (38, 39). Further experiments will need to be conducted to provide a definite molecular link between p53 and p21 in ERK5-deficient macrophages, given that p21 can be induced via both p53-dependent and -independent mechanisms (40). For example, we have previously proposed that ERK5 blocked p21 upregulation through c-Myc-dependent transcriptional regulation of *miR-17-5p* and *miR-20a* in breast cancer cells (41). Moreover, in light of previous evidence that p21 was crucial for the maturation and differentiation of macrophages (24, 25), we anticipate that ERK5 supports macrophage proliferation through blocking differentiation, rather than having a direct effect on the cell cycle. This model is consistent with our demonstration that ERK5-deficient monocytes/macrophages exhibiting a high level of p21 differentiated more rapidly. The requirement of ERK5 to regulate the level of p21 might also be responsible for causing increased STAT3 signaling and the acquisition of protumorigenic TAM phenotypes (8, 42).

Mechanistically, the ability of ERK5 to block macrophage differentiation might involve decreased expression of transcription factors of the Maf family, given that *cMaf/MafB* deficiency rendered functionally differentiated macrophages capable of expanding through self-renewal via KLF4 and c-Myc (43). Consistently, a further analysis demonstrated that transient downregulation of Maf transcription factors was required for proliferating resident macrophages (44). Moreover, both KLF4 and c-Myc, which have been implicated in pluripotent stem cell reprogramming (45), are ERK5 targets (46, 47). However, a recent study showed that cMaf was a transcriptional regulator of protumoral macrophage activation (48). In the future, unbiased transcriptomic studies to establish the transcriptional network downstream of ERK5 will be essential to understand how ERK5 maintains proliferative protumor macrophage populations to support tumor progression and malignancy. In particular, these data will clarify the requirement of Maf factors downstream of ERK5 and may reveal potential important functional cross talks between p21, Maf, and STAT3 implicated in protumoral macrophage polarization.

In summary, we demonstrate in this study that TAM proliferation is a general mechanism in cancer. Moreover, we provide a novel insight into TAM self-renewal with the potential clinical implication of pharmacologic inhibition of ERK5, alone or combined with other therapeutic strategies based on blocking the survival or the recruitment of macrophages (49), to achieve long-term control of malignancy and endure remission for patients with cancer.

Disclosure of Potential Conflicts of Interest

N. Gray reports personal fees from Syros, Petra, C4 Therapeutics, Aduro, B2S, Gatekeeper, Soltego, Jengu, and Allorion, as well as grants from Deerfield, Taiho, and Takeda outside the submitted work; and Nathanael Gray is a founder, science advisory board member (SAB), and equity holder in Gatekeeper, Syros, Petra, C4, B2S, Aduro, Allorion, Jengu, and Soltego (board member). The Gray lab receives or has received research funding from Novartis, Takeda, Astellas, Taiho, Janssen, Kinogen, Voronoi, Arbella, Deerfield, and Sanofi. No potential conflicts of interest were disclosed by the other authors.

Authors' Contributions

E. Giurisato: Conceptualization, formal analysis, supervision, investigation, visualization, methodology and writing-original draft. **S. Lonardi:** Investigation, visualization and methodology. **B. Telfer:** Investigation and methodology. **S. Lussoso:** Investigation. **B. Risa-Ebrí:** Investigation. **J. Zhang:** Investigation. **I. Russo:** Resources, formal analysis and investigation. **J. Wang:** Resources. **A. Santucci:** Resources. **K.G. Finegan:** Resources and funding acquisition. **N.S. Gray:** Resources. **W. Vermi:** Resources, formal analysis, supervision and visualization. **C. Tournier:** Conceptualization, supervision, funding acquisition, visualization, writing-review and editing.

Acknowledgments

This work was supported by grants mainly from Worldwide Cancer Research to Cathy Tournier and partly from the Medical Research Council Confidence in Concept (CiC7) scheme to K. Finegan, and by a Marie Curie Research Fellowship to E. Giurisato. S. Lussoso was supported by Fondazione Beretta and W. Vermi was supported by Associazione Italiana per la Ricerca sul Cancro (IG grant no. 15378). We are grateful to Sara Licini and Debora Bresciani (supported by Fondazione Beretta) for their excellent support on preparation of human tissue biopsies and image processing. We thank Michael Cross for providing adenovirus particles expressing caMEK5 and ERK5. We thank Peter March and Peter Walker (Bioimaging and Histology Facilities, University of Manchester) for very helpful advice and the staff at the University of Manchester Biological Safety Unit for looking after the mice.

The costs of publication of this article were defrayed in part by the payment of page charges. This article must therefore be hereby marked *advertisement* in accordance with 18 U.S.C. Section 1734 solely to indicate this fact.

Received August 5, 2019; revised April 7, 2020; accepted June 12, 2020; published first June 19, 2020.

References

1. Allavena P, Sica A, Solinas G, Porta C, Mantovani A. The inflammatory microenvironment in tumour progression: the role of tumour-associated macrophages. Crit Rev Oncol Hematol 2008;66:1–9.
2. Noy R, Pollard JW. Tumor-associated macrophages: from mechanisms to therapy. Immunity 2014;41:49–61.
3. Ruffell B, Coussens LM. Macrophages and therapeutic resistance in cancer. Cancer Cell 2015;27:462–72.
4. Komohara Y, Jinushi M, Takeya M. Clinical significance of macrophage heterogeneity in human malignant tumors. Cancer Sci 2014;105:1–8.
5. Bingle L, Brown NJ, Lewis CE. The role of tumour-associated macrophages in tumour progression: implications for new anticancer therapies. J Pathol 2002;196:254–65.
6. Cassetta L, Pollard A. Targeting macrophages: therapeutic approaches in cancer. Nat Rev Drug Discov 2018;17:887–904.
7. Mantovani A, Marchesi F, Malesci A, Laghi L, Allavena P. Tumour-associated macrophages as treatment targets in oncology. Nat Rev Clin Oncol 2017;14:399–416.
8. Giurisato E, Xu Q, Lonardi S, Telfer B, Russo I, Pearson A, et al. Myeloid ERK5 deficiency suppresses tumour growth by blocking protumour macrophage polarization via STAT3 inhibition. Proc Natl Acad Sci U S A 2018;115:E2801–10.
9. Nithianandarajah-Jones GN, Wilm B, Goldring CE, Muller J, Cross MJ. ERK5: structure, regulation and function. Cell Signal 2012;24:2187–96.
10. Hayashi M, Lee JD. Role of the BMK1/ERK5 signaling pathway: lessons from knockout mice. J Mol Med 2004;82:800–8.
11. Movahedi K, Laoui D, Gyseman C, Baeten M, Stangè G, Van den Bossche J, et al. Different tumor microenvironments contain functionally distinct subsets of macrophages derived from Ly6C(high) monocytes. Cancer Res 2010;70:5728–39.
12. Qian BZ, Li J, Zhang H, Kitamura T, Zhang J, Campion LR, et al. CCL2 recruits inflammatory monocytes to facilitate breast-tumour metastasis. Nature 2011;475:222–5.
13. Franklin RA, Liao W, Sarkar A, Kim MV, Bivona MR, Liu K, et al. The cellular and molecular origin of tumor-associated macrophages. Science 2014;344:921–5.
14. Bowman RL, Klemm F, Akkari L, Pyonteck SM, Sevenich L, Quail DF, et al. Macrophage ontogeny underlies differences in tumor-specific education in brain malignancies. Cell Rep 2016;17:2445–59.

15. Franklin RA, Li MO. Ontogeny of tumor-associated macrophages and its implication in cancer regulation. Trends Cancer 2016;2:20–34.
16. Evans R, Cullen RT. In situ proliferation of intratumor macrophages. J Leukoc Biol 1984;35:561–72.
17. Bottazzi B, Erba E, Nobili N, Fazioli F, Rambaldi A, Mantovani A. A paracrine circuit in the regulation of the proliferation of macrophages infiltrating murine sarcomas. J Immunol 1990;144:2409–12.
18. Campbell MJ, Tonlaar NY, Garwood ER, Huo D, Moore DH, Khramtsov AI, et al. Proliferating macrophages associated with high grade, hormone receptor negative breast cancer and poor clinical outcome. Breast Cancer Res Treat 2011; 128:703–11.
19. Tymoszuk P, Evens H, Marzola V, Wachowicz K, Wasmer MH, Datta S, et al. In-situ proliferation contributes to accumulation of tumor-associated macrophages in spontaneous mammary tumors. Eur J Immunol 2014;44:2247–62.
20. Zhu Y, Herndon JM, Sojka DK, Kim KW, Knolhoff BL, Zuo C, et al. Tissue-resident macrophages in pancreatic ductal adenocarcinoma originate from embryonic hematopoiesis and promote tumour progression. Immunity 2017; 47:323–38.
21. Chitu V, Stanley ER. Colony-stimulating factor-1 in immunity and inflammation. Curr Opin Immunol 2006;18:39–48.
22. Rovida E, Spinelli E, Sdelci S, Barbetti V, Morandi A, Giuntoli S, et al. ERK5/BMK1 is indispensable for optimal colony-stimulating factor 1 (CSF-1)-induced proliferation in macrophages in a Src-dependent fashion. J Immunol 2008;180: 4166–72.
23. Wang X, Pesakhov S, Harrison JS, Kafka M, Danilenko M, Studzinski GP. The MAPK ERK5, but not ERK1/2, inhibits the progression of monocytic phenotype to the functioning macrophage. Exp Cell Res 2015;330:199–211.
24. Asada M, Yamada T, Ichijo H, Delia D, Miyazono K, Fukumuro K, et al. Apoptosis inhibitory activity of cytoplasmic p 21(Cip1/WAF1) in monocytic differentiation. EMBO J 1999;18:1223–34.
25. Kramer JL, Baltathakis I, Alcantara OS, Boldt DH. Differentiation of functional dendritic cells and macrophages from human peripheral blood monocyte precursors is dependent on expression of p21 (WAF1/CIP1) and requires iron. Br J Haematol 2002;117:727–34.
26. Williams CA, Fernandez-Alonso R, Wang J, Toth R, Gray NS, Findlay GM. Erk5 is a key regulator of naive-primed transition and embryonic stem cell identity. Cell Rep 2016;16:1820–8.
27. Misharin AV, Morales-Nebreda L, Mutlu GM, Budinger GR, Perlman H. Flow cytometric analysis of macrophages and dendritic cell subsets in the mouse lung. Am J Respir Cell Mol Biol 2013;49:503–10.
28. Qian B, Deng Y, Im JH, Muschel RJ, Zou Y, Li J, et al. A distinct macrophage population mediates metastatic breast cancer cell extravasation, establishment and growth. PLoS One 2009;4:e6562.
29. Zhu XD, Zhang JB, Zhuang PY, Zhu HG, Zhang W, Xiong YQ, et al. High expression of macrophage colony-stimulating factor in peritumoral liver tissue is associated with poor survival after curative resection of hepatocellular carcinoma. J Clin Oncol 2008;26:2707–16.
30. Ries CH, Hoves S, Cannarile MA, Rüttinger D. CSF-1/CSF-1R targeting agents in clinical development for cancer therapy. Curr Opin Pharmacol 2015;23:45–51.
31. Patsialou A, Wyckoff J, Wang Y, Goswami S, Stanley ER, Condeelis JS. Invasion of human breast cancer cells in vivo requires both paracrine and autocrine loops involving the colony-stimulating factor-1 receptor. Cancer Res 2009;69:9498–506.
32. Lin EY, Nguyen AV, Russell RG, Pollard JW. Colony-stimulating factor 1 promotes progression of mammary tumors to malignancy. J Exp Med 2001; 193:727–40.
33. Paulus P, Stanley ER, Schafer R, Abraham D, Aharinejad S. Colony-stimulating factor-1 antibody reverses chemoresistance in human MCF-7 breast cancer xenografts. Cancer Res 2006;66:4349–56.
34. Sieweke MH, Allen JE. Beyond stem cells: self-renewal of differentiated macrophages. Science 2013;342:1242974.
35. Bonapace L, Coissieux MM, Wyckoff J, Mertz KD, Varga Z, Junt T, et al. Cessation of CCL2 inhibition accelerates breast cancer metastasis by promoting angiogenesis. Nature 2014;515:130–3.
36. Mäkitie T, Summanen P, Tarkkanen A, Kivelä T. Tumor-infiltrating macrophages (CD68(+) cells) and prognosis in malignant uveal melanoma. Invest Ophthalmol Vis Sci 2001;42:1414–21.
37. Smith MP, Sanchez-Laorden B, O'Brien K, Brunton H, Ferguson J, Young H, et al. The immune microenvironment confers resistance to MAPK pathway inhibitors through macrophage-derived TNFα. Cancer Discov 2014;4:1214–29.
38. Yang Q, Deng X, Lu B, Cameron M, Fearns C, Patricelli MP, et al. Pharmacological inhibition of BMK1 suppresses tumor growth through promyelocytic leukemia protein. Cancer Cell 2010;18:258–67.
39. Yang Q, Liao L, Deng X, Chen R, Gray NS, Yates JR 3rd, et al. BMK1 is involved in the regulation of p53 through disrupting the PML-MDM2 interaction. Oncogene 2013;32:3156–64.
40. El-Deiry WS. p21(WAF1) mediates cell-cycle inhibition, relevant to cancer suppression and therapy. Cancer Res 2016;76:5189–91.
41. Perez-Madrigal D, Finegan KG, Paramo B, Tournier C. The extracellular-regulated protein kinase 5 (ERK5) promotes cell proliferation through the down-regulation of inhibitors of cyclin dependent protein kinases (CDKs). Cell Signal 2012;24:2360–8.
42. Coqueret O, Gascan H. Functional interaction of STAT3 transcription factor with the cell cycle inhibitor p21WAF1/CIP1/SDI1. J Biol Chem 2000;275: 18794–800.
43. Aziz A, Soucie E, Sarrazin S, Sieweke MH. MafB/c-Maf deficiency enables self-renewal of differentiated functional macrophages. Science 2009;326:867–71.
44. Soucie EL, Weng Z, Geirsdóttir L, Molawi K, Maurizio J, Fenouil R, et al. Lineage-specific enhancers activate self-renewal genes in macrophages and embryonic stem cells. Science 2016;351:aad5510.
45. Takahashi K, Tanabe K, Ohnuki M, Narita M, Ichisaka T, Tomoda K, et al. Induction of pluripotent stem cells from adult human fibroblasts by defined factors. Cell 2007;131:861–72.
46. Ohnesorge N, Viemann D, Schmidt N, Czymai T, Spiering D, Schmolke M, et al. Erk5 activation elicits a vasoprotective endothelial phenotype via induction of Kruppel-like factor 4 (KLF4). J Biol Chem 2010;285:26199–210.
47. English JM, Pearson G, Baer R, Cobb MH. Identification of substrates and regulators of the mitogen-activated protein kinase ERK5 using chimeric protein kinases. J Biol Chem 1998;273:3854–60.
48. Liu M, Tong Z, Ding C, Luo F, Wu S, Wu C, et al. Transcription factor c-Maf is a checkpoint that programs macrophages in lung cancer. J Clin Invest. 2020;130: 2081–96.
49. Majety M, Runza V, Lehmann C, Hoves S, Ries CH. A drug development perspective on targeting tumor-associated myeloid cells. FEBS J. 2018; 285: 763–76.

Cancer Research
The Journal of Cancer Research (1916–1930) | The American Journal of Cancer (1931–1940)

AACR American Association for Cancer Research

Extracellular-Regulated Protein Kinase 5-Mediated Control of p21 Expression Promotes Macrophage Proliferation Associated with Tumor Growth and Metastasis

Emanuele Giurisato, Silvia Lonardi, Brian Telfer, et al.

Cancer Res 2020;80:3319-3330. Published OnlineFirst June 19, 2020.